Parametric decay instabilities in the HELIX helicon plasma source

J. L. Kline
Los Alamos National Laboratory, Los Alamos, New Mexico 87545

E. E. Scime[a)]
Physics Department, West Virginia University, Morgantown, West Virginia 26506

(Received 13 June 2002; accepted 7 October 2002)

Parametric decay of the electromagnetic helicon pump wave into two electrostatic waves, thought to be a lower hybrid wave and an ion acoustic wave, is observed. The parametric excitation of the electrostatic waves is strongest near the axis of the helicon source. The parametrically excited wave amplitudes can be as large as 8% of the pump wave amplitude. Thus, efficient coupling between the parametrically excited waves and plasma particles (ions and electrons) can lead to enhanced plasma densities, electron temperatures, and ion temperatures. A correlation between the lower hybrid wave and electron temperatures and a correlation between the ion acoustic wave and ion temperatures near the antenna are observed. © *2003 American Institute of Physics.* [DOI: 10.1063/1.1528182]

I. INTRODUCTION

There are many unanswered questions concerning density production, ion heating, and damping of the helicon wave in helicon sources. Even if recently proposed general theories concerning rf power absorption in helicon sources (see, for example, Ref. 1) are validated by additional experiments, questions about how other linear and nonlinear microprocesses can alter the general characteristics of helicon sources will remain. For instance, Light *et al.*[2] suggest that the excitation of unstable low-frequency waves in helicon sources leads to anomalous particle transport and a constant or decreasing plasma density at high magnetic field strengths even though most general helicon source theories predict an increasing density with increasing magnetic field strength. The theoretical prediction of Akhiezer *et al.*[3] that electron **E×B** drifts in the helicon wave fields can excite parametric sound turbulence that heats electrons via nonlinear scattering is another example of a plasma process outside the scope of most helicon source models.

In fusion plasmas, it has long been established that parametric instabilities occur during rf heating of particles.[4–7] The parametric instabilities can reduce the efficiency of the rf heating if the pump wave is responsible for heating the particles by reducing the amplitude of the pump wave. However, the parametrically excited waves can also heat the particles. Therefore, parametric decay of the pump wave can also result in improved particle heating. Because helicon sources have a large amplitude rf wave propagating along the axis of the discharge, it should not be surprising that parametric decay of the rf pump wave can occur in helicon sources. In fact, Boswell studied parametric decay of whistler waves in rf generated plasma sources in the 1970s.[8] For helicon sources, parametrically excited waves provide an alternative mechanism for the helicon wave to interact with the particles. Typically, the phase speed of the helicon wave is much larger than the thermal speed of both the ions and electrons. However, the phase speed of the parametrically excited waves can be comparable to the electron or the ion thermal speed. Thus, energy from the helicon wave can be converted to particle kinetic energy through linear or nonlinear damping of the parametrically excited waves.

In this paper, experimental evidence of parametrically coupled electrostatic waves is presented for the HELIX helicon source experiment operating in the eight-coil configuration. The characteristics of the coupled electrostatic waves, e.g., wave number, dependence on rf power, radial variations, and dependence on rf and magnetic field strength, are investigated. Measurements of the electromagnetic wave spectrum are also presented confirming that the parametrically driven waves in HELIX are purely electrostatic.

The experimental data suggest that the rf pump wave parametrically drives an electrostatic lower hybrid wave and a low frequency ion acoustic wave. Correlations between the amplitude of the lower hybrid wave and the electron temperature and the amplitude of the ion acoustic wave and the ion temperature near the antenna are reviewed in Sec. V of this work. The effects of parametrically driven waves on energy coupling into helicon sources are discussed in Sec. VI.

II. EXPERIMENTAL APPARATUS

The Hot hELIcon eXperiment (HELIX) vacuum chamber is a 61 cm long, Pyrex tube 10 cm in diameter connected to a 91 cm long, stainless steel chamber that is 15 cm in diameter (see Fig. 1). The stainless steel chamber has one set of four 6'' Conflat™ crossing ports in the center of the chamber and two sets of four $2\frac{3}{4}$'' Conflat™ crossing ports on either side that are used for diagnostic access. The opposite end of the stainless steel chamber opens into a 2 m diameter space chamber, the Large Experiment on Instabilities and Anisotropies (LEIA).[9] Ten electromagnets typically produce a steady-state axial magnetic field of 0–1200 Gauss. However, for these experiments, only eight electromagnets were used so that the peak magnetic field could be increased to 1320 Gauss.[10] The source gas is argon at neutral pressures of

a)Electronic mail: escime@wvu.edu

 © 2003 American Institute of Physics

Downloaded 19 Dec 2002 to 157.182.108.189. Redistribution subject to AIP license or copyright, see http://ojps.aip.org/pop/popcr.jsp

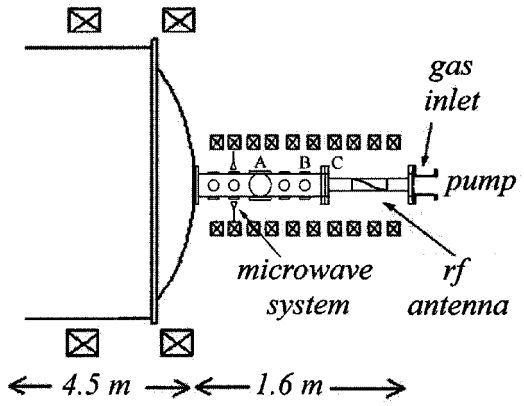

FIG. 1. Schematic diagram of HELIX and LEIA plasma chambers with diagnostic placement.

1–10 mTorr. RF power of up to 2.0 kW over a frequency range of 6–18 MHz is used to create the steady-state plasma. A 19 cm, half wave, right-handed helix antenna is used to generate the plasma. The right-handedness is relative to the magnetic-field direction, and is designed to launch the $m=+1$ helicon wave towards LEIA. Characteristic electron temperatures and densities in HELIX are $T_e \approx 4$ eV and $n \geqslant 1\times 10^{13}$ cm^3 measured with an rf compensated Langmuir probe.[11] For all the experiments reported here, the magnetic field in LEIA was fixed at 36 Gauss.

The ion temperatures, both parallel and perpendicular, were obtained from direct measurements of the ion velocity space distribution with laser induced fluorescence (LIF).[12,13] A Coherent 899 ring dye laser pumps the $(3d')^2G_{9/2}$ metastable argon ion line to the $(4p')^2F^0_{7/2}$ state which then decays via emission of the 461 nm photon to the $(4s')^2D_{5/2}$ state. As the laser frequency, centered on a wavelength of 611.5 nm, was swept through 10 GHz, the fluorescent emission from the pumped upper level was measured with a filtered photomultiplier tube detector. A curve fit to the Doppler broadened absorption linewidth was used to determine the ion temperature.[14,15] All the perpendicular ion temperature measurements referred to in this work were performed at the axial position labeled "C" in Fig. 1.

Magnetic and electrostatic fluctuation measurements were accomplished with pairs of probes at axial position "B" in Fig. 1. The magnetic fluctuation probe consisted of five sense coils (approximately 175 turns of 40 gauge wire per 1.3 mm OD by 1.3 mm long coil) housed within a 25.4 mm diameter, boron nitride shield. The five sense coils formed a cross pattern (+) with the axes of all five coils in the same direction. The axes of the sense coils were 6.35 mm from the end of the boron nitride housing. The boron nitride housing was mounted on a probe shaft that could move radially across the plasma. The shaft could also be rotated to measure magnetic fluctuations parallel (z direction) and perpendicular (azimuthal direction) to the applied magnetic field. With the cross pattern, simultaneous phase difference measurements of the same magnetic-field component could be measured in two orthogonal directions.[10] The two ends of the sense coils were connected across one side of a center-tapped, one-to-one transformer inside the probe shaft. The transformers were placed as close to the coils as possible to eliminate electrostatic pick-up.[16,17] The electrostatic probe consisted of two Langmuir probe tips separated by 3.2 mm.[10] So that high-frequency floating potential fluctuations could be measured, the electrostatic probe tips were not rf compensated.

Wave numbers were calculated from the measured phase differences between both the magnetic sense coils and the electrostatic probe tips using a fixed pair probe analysis technique.[18] The phase difference and fluctuation power as a function of frequency was determined from the cross-power spectrum of time series from two probe tips or sense coils. The cross power spectrum, $P_{12}(\Delta x,\omega)$, is defined as

$$P_{12}(\Delta x,\omega)=\Phi_1(x_1,\omega)\Phi_2^*(x_2,\omega), \tag{1}$$

where $\Phi_1(x_1,\omega)$ is the fast Fourier transform (FFT) of the time series from probe one, $\Phi_2^*(x_2,\omega)$ is the complex conjugate of the FFT of time series from probe two, and Δx is the spatial separation between the two measurement locations. Writing the cross-power spectrum in real and imaginary components

$$P_{12}(\Delta x,\omega)=(\varphi_{1\,\mathrm{Re}}\varphi_{2\,\mathrm{Re}}+\varphi_{2\,\mathrm{Im}}\varphi_{1\mathrm{Im}}) + i(\varphi_{2\,\mathrm{Re}}\varphi_{1\mathrm{Im}}-\varphi_{2\,\mathrm{Im}}\varphi_{1\,\mathrm{Re}}), \tag{2}$$

the phase of the complex cross-power spectrum becomes

$$\Theta(\omega)=\tan^{-1}\left(\frac{(\varphi_{2\,\mathrm{Re}}\varphi_{1\mathrm{Im}}-\varphi_{2\,\mathrm{Im}}\varphi_{1\,\mathrm{Re}})}{(\varphi_{1\,\mathrm{Re}}\varphi_{2\,\mathrm{Re}}+\varphi_{2\,\mathrm{Im}}\varphi_{1\mathrm{Im}})}\right). \tag{3}$$

From Eq. (3), the wave number for each frequency step of the FFT can be calculated by dividing by the probe separation distance, Δx. Although the wave numbers at wave frequencies with large wave amplitudes can be obtained from a single pair of filtered time series, in turbulent plasma conditions or when waves have a small signal to noise ratio, an ensemble average of multiple cross-power spectra provides a more complete picture of the spectrum of wave frequencies and wave numbers.

To create the ensemble averaged spectrum, a two-dimensional matrix of frequency versus wave number is created. The average power for each frequency, $\frac{1}{2}(P_1(x_1,\omega)+P_2(x_2,\omega))/M$ (where M is the number of time records), is placed in the appropriate wave number bin calculated from Eq. (3). This is repeated for multiple time records. In this work, 84 sets of time records were used. For random signals, the average power will be small and the wave numbers spread out over the whole wave number spectrum. For periodic signals, the average power will be large and the wave numbers will have a finite width. The values in the frequency and wave number bins for these signals become larger than those of random signals increasing the signal to noise. Since the ensemble averaged spectrum is a compilation from multiple time records, turbulent or time-dependent waves with a finite frequency and/or wave number range can be detected. This is the key advantage of the ensemble averaged, digital cross-power spectral analysis method.

Although the fixed probe pair analysis detects turbulent waves, there are limitations to the measurement. The maximum and minimum measurable frequency is determined by the typical limits of the FFT. As for the wave numbers, there

Downloaded 19 Dec 2002 to 157.182.108.189. Redistribution subject to AIP license or copyright, see http://ojps.aip.org/pop/popcr.jsp

are two limits. Mathematically, the minimum measurable wave number is a function of the number of data records in the time series, N, and the probe separation distance, $k_{\min}=2\pi/\Delta xN$. For all of the measurements reported here, each time series was 8192 points long and the mathematical limit is much smaller than the physical limits of the probe and data acquisition system. The minimum resolvable wave number was estimated to be $k_{\min}\approx 0.05$ rad/cm. The second limit is a physical limit attributed to the probe separation. If the wavelength is shorter than the separation distance between the two probes, aliasing of the wave number occurs, i.e., the probe cannot differentiate between ϕ and $\phi+2\pi n$ where n is an integer. The criteria are further restricted if the propagation direction of the wave is not known. The difference between $3\pi/2$ and $-\pi/2$ cannot be determined by the probe measurements. Since the propagation direction of the waves is unknown, the phase measurements are restricted to the range $\pi/2$ to $-\pi/2$, limiting the minimum measurable wavelength to twice the probe separation distance, $2\Delta x$. Thus, the minimum measurable wavelength for the electrostatic probe is restricted to 6.4 mm or a wave number range of ± 9.8 rad/cm. Positive wave numbers represent waves propagating parallel to the applied magnetic field and waves propagating in the right hand direction with respect to the applied magnetic field. To ensure that the measured wave numbers were not aliased, i.e., wavelengths smaller $2\Delta x$, wave number measurements were made at multiple probe angles with respect to the applied magnetic field. The perpendicular wave number at the various angles remained the same. If the wave numbers had been aliased, the perpendicular wave number would have changed as a function of angle as the phase difference went from ϕ to $\phi+2\pi$.

III. EXPERIMENTAL MEASUREMENTS OF PARAMETRIC DECAY

The standard criteria for establishing that three waves are parametrically coupled are the two matching conditions, energy conservation and momentum conservation, described by $\omega_o=\omega_1\pm\omega_2$ and $k_o=k_1\pm k_2$. Figure 2 shows the spectral amplitude of the electric field fluctuations at a radius of 2 cm for a pump frequency of 11 MHz, a magnetic-field strength of 845 Gauss, a neutral pressure of 6.7 mTorr, and an rf power of 750 Watts. Clear energy conservation is established with the pump wave decaying into two side bands and a low-frequency mode as indicated in the figure. The wave amplitude for the lower side band is about 8% of the pump electric field and is the largest measured in these experiments. Figure 3 shows the frequency spectrum of magnetic-field fluctuations parallel to the magnetic field at a radius of 2 cm as measured by a single magnetic sense coil for the same parameters and acquired at the same location as the data shown in Fig. 2. The electromagnetic fluctuation spectrum shows no sign of parametric decay as only the pump wave has an electromagnetic signature. Measurements of the azimuthal magnetic field were also made and showed no sign of parametric decay. The residual small peak in the spectrum near 9.5 MHz is due to a large resonance in the magnetic sense coil at 9.5 MHz.[10] Since the electric field fluctuations

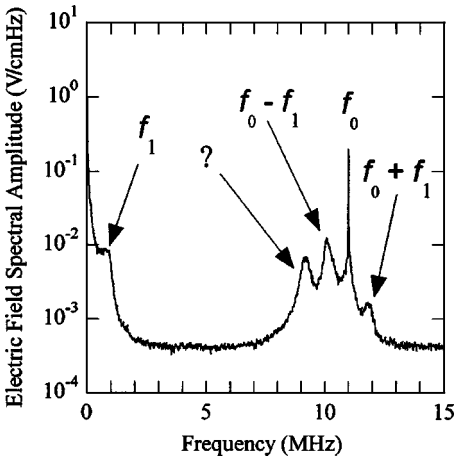

FIG. 2. Electrostatic fluctuation spectrum at a radius of 2 cm for an rf of 11 MHz, a neutral pressure of 6.7 mTorr, an rf power of 750 Watts, and a magnetic-field strength of 845 Gauss. The upper and lower side band peaks are displaced from the rf pump frequency by the same frequency as the low-frequency wave.

of the parametrically exited waves were measured both in the azimuthal and the parallel direction relative to the applied magnetic field, a magnetic component of the excited waves would have been measured in the azimuthal or parallel direction if the waves were electromagnetic. Thus, the electromagnetic frequency spectrum indicates that the three parametrically excited waves (two sideband and one low frequency) are purely electrostatic. All other parametrically excited waves discussed in this work were also found to be purely electrostatic. As a quick check of the electromagnetic fluctuation measurements, the area under the pump wave was integrated yielding a magnetic-field fluctuation amplitude of 5.9 Gauss; consistent with other measurements of the amplitude of the helicon wave in helicon sources.[19]

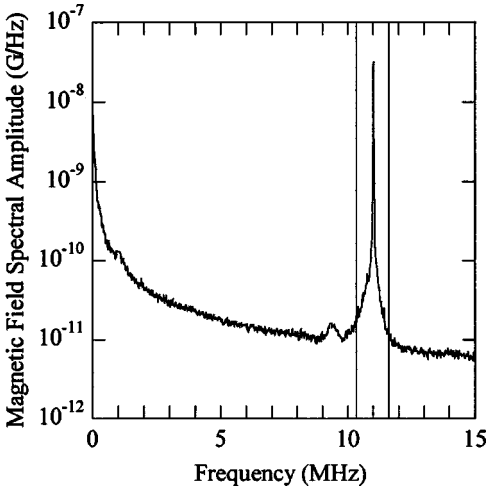

FIG. 3. Frequency spectrum of magnetic-field fluctuations along the magnetic field (z direction) at a radius of 2 cm for an rf of 11 MHz, a neutral pressure of 6.7 mTorr, an rf power of 750 Watts, and a magnetic-field strength of 845 Gauss. No sidebands or low-frequency waves are apparent. Integration of the area under the curve between the two vertical lines yields a magnetic-field strength of 5.9 Gauss for the pump wave.

Downloaded 19 Dec 2002 to 157.182.108.189. Redistribution subject to AIP license or copyright, see http://ojps.aip.org/pop/popcr.jsp

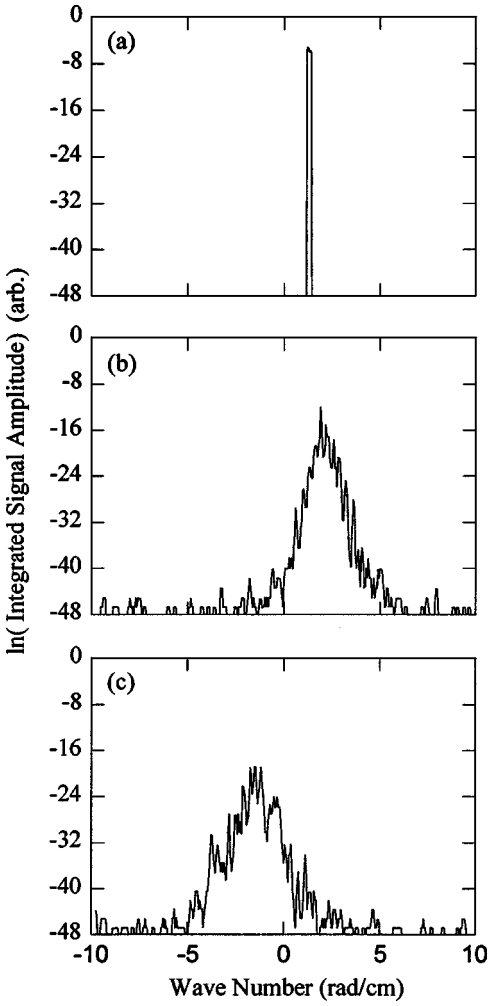

FIG. 4. Natural logarithm of the electrostatic spectral power integrated over 70 kHz around the central wave frequency versus wave number for the (a) pump wave, (b) low frequency wave, and (c) lower side band wave propagating along the applied magnetic field.

The electrostatic fluctuation power spectrum also includes an additional electrostatic wave around $f \sim 9$ MHz that has yet to be identified. The 9 MHz wave does not change frequency with magnetic-field strength, rf driving frequency, or plasma density. The electrostatic fluctuation spectrum was measured with two different digitizers at two different digitization rates and identical results were obtained.[20] Because background test measurements (with all apparatus turned on but without argon gas in the plasma chamber) show no evidence of the anomalous 9 MHz wave, the wave either truly exists in the plasma or results from an electrical resonance in the electrostatic probe-digitizer measurement circuit. Although we continue to seek to understand the origins of the 9 MHz peak, in the remainder of this work the 9 MHz peak is not discussed as it is not coupled to the other waves observed in the experiment.

Parametric coupling also requires that momentum be conserved among the sideband, pump, and low-frequency waves. The wave number spectrum, obtained from the two tips of the electrostatic probe, for the low frequency wave, the lower sideband (LSB), and the pump waves shown in Fig. 2 are shown in Fig. 4 for wave propagation along the applied magnetic field. The sum of the wave numbers is zero to within the experimental error: $k_{lf} \sim 2.1 \pm 0.2$ rad/cm for the low frequency component, $k_{\mathrm{LSB}} \sim -1.5 \pm 0.3$ rad/cm for the lower side band, and $k_p \sim 1.0 \pm 0.1$ rad/cm for the pump. The statistical error in the wave number measurements is the error in the mean based on 84 measurements at each frequency. Although the mean wave number is known with good precision, Fig. 4 also shows that the standard deviation, Δk, is much larger, i.e., on the order of $\Delta k \sim 1.5$ rad/cm. Thus it appears that the parametric decay processes in HELIX generate a turbulent wave spectrum. Nonetheless, these wave number measurements demonstrate that the two conditions required to demonstrate parametric coupling, energy and momentum conservation, are satisfied in these HELIX plasmas.

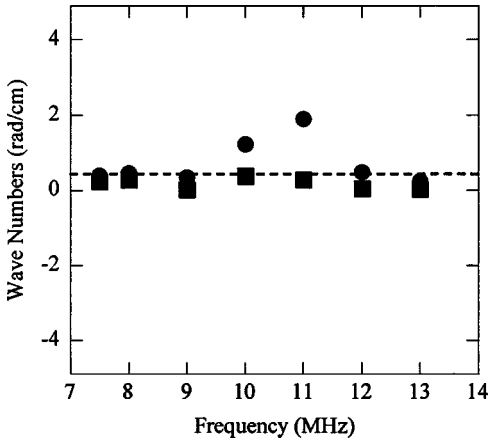

FIG. 5. (■) Azimuthal and (●) parallel electrostatic wave number of the pump wave versus rf for a magnetic-field strength of 845 Gauss, a neutral pressure of 6.7 mTorr, and an rf power of 750 Watts. The dashed line indicates the azimuthal wave number expected for a $m = +1$ wave.

A. Wave number versus pump frequency

The parallel and azimuthal wave numbers of the pump wave versus rf measured at a radius of 2 cm are shown in Fig. 5 for a magnetic-field strength of 845 Gauss, a neutral pressure of 6.7 mTorr, and an rf power of 750 Watts. Except at 10 and 11 MHz, the parallel wave numbers for the pump wave are on the order of $k_{\parallel} \sim 0.4$ rad/cm, i.e., parallel wavelengths of approximately 16 cm. The most likely source of an approximately 16 cm long electrostatic wave at the rf is the 19 cm long rf antenna. However, at 10 and 11 MHz, the parallel wavelength of the pump wave suddenly decreases to approximately 6 and 3 cm, respectively. The measurements indicate a fundamental change in the nature of the electrostatic wave at the pump frequency at these two frequencies. At typical HELIX densities and a magnetic-field strength of 845 Gauss, the lower hybrid frequency

$$1/\omega_{\mathrm{lh}}^2 = 1/(\omega_{\mathrm{ce}}\omega_{\mathrm{ci}}) + 1/(\omega_{\mathrm{pi}}^2 + \omega_{\mathrm{ci}}^2), \tag{4}$$

where ω_{lh} is the lower hybrid frequency, ω_{ci} is the ion cyclotron frequency, ω_{ce} is the electron cyclotron frequency, and ω_{pi} is the ion plasma frequency, is approximately 9 MHz near the axis of the source. Therefore, when the rf is just above the lower hybrid frequency, the parallel wavelength of the electrostatic wave at the pump frequency decreases

Downloaded 19 Dec 2002 to 157.182.108.189. Redistribution subject to AIP license or copyright, see http://ojps.aip.org/pop/popcr.jsp

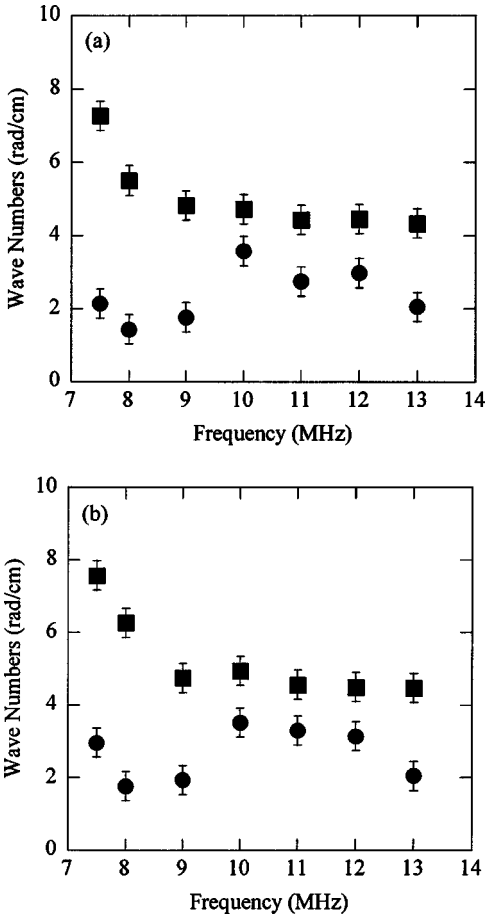

FIG. 6. (■) Azimuthal and (●) parallel electrostatic wave number of the (a) upper side band and (b) low-frequency waves versus rf for a magnetic-field strength of 845 Gauss, a neutral pressure of 6.7 mTorr, and an rf power of 750 Watts.

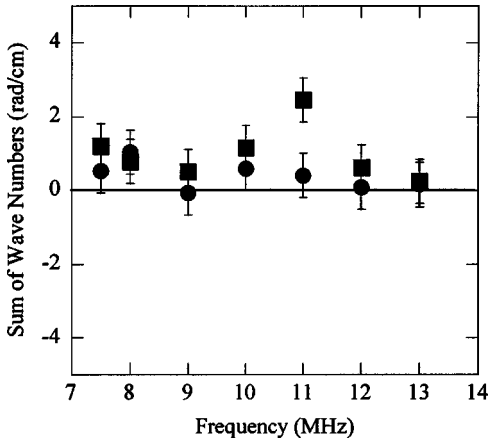

FIG. 7. The sum, $k_{rf}+k_{USB}-k_{lf}$, of the (■) azimuthal and (●) parallel electrostatic wave numbers for the rf pump, upper side band, and low-frequency electrostatic waves versus rf pump frequency. The upper side band waves were always approximately 400–800 kHz away from the pump frequency and the low-frequency waves were always in the range of 400–800 kHz.

sharply. As reported elsewhere, the nature of ion heating in HELIX changes dramatically when the rf is equal to the local lower hybrid frequency.[15,20] Note that the azimuthal wave number is typically much smaller than what would be expected for a $|m|=1$ wave propagating azimuthally at $r=2$ cm ($k_\theta \sim 0.5$ rad/cm). In fact, at the highest pump frequencies, the electrostatic wave at the pump frequency is an $m=0$, azimuthally symmetric wave.

At $r=2$ cm, the azimuthal (perpendicular) wave numbers for the upper side band (USB) wave [see Fig. 6(a)] start at $k_\theta=7.5$ rad/cm and decrease (in magnitude) to about $k_\theta=5.0$ rad/cm at an rf of 9 MHz. Above 9 MHz, i.e., above the local lower hybrid frequency, there is almost no change in the azimuthal wave number with rf. The azimuthal wave number data between 7.5 and 9.0 MHz have the unique signature of a backward propagating wave. Keeping in mind that the frequency of the upper side band wave for these plasma parameters was always a constant 400–800 kHz above the rf of the pump wave, the phase velocity, ω/k_θ, of the upper side band wave is negative while the group velocity, $d\omega/dk_\theta$ is positive, i.e., backwards propagation. Backward propagation is characteristic of electrostatic lower hybrid waves.[21,22] Thus, for rf below 9 MHz, the upper side band wave can be identified as an electrostatic lower hybrid wave. Similar measurements of the lower side band indicate that it is also electrostatic lower hybrid wave for rf below 9 MHz for a magnetic-field strength of 845 Gauss.

Both the parallel and azimuthal wave numbers for the low-frequency wave track the upper side band wave numbers as a function of rf [Fig. 6(b)]. The near one-to-one correspondence between the low-frequency wave numbers and upper side band wave numbers is due to the momentum conservation parametric coupling condition and the small wave number magnitudes of the pump wave. The wave number sum, $k_{rf}+k_{USB}-k_{lf}$, is plotted in Fig. 7 as a function of the rf pump frequency (not the actual electrostatic wave frequencies). The parallel wave numbers are conserved for all frequencies. However, the perpendicular wave numbers are clearly not conserved at 10 and 11 MHz or below 8 MHz. Since the group velocity for both of the parametrically excited waves is in the same direction, the parametric instability is a convective instability.[23,24] Therefore, it is possible to obtain a wave number mismatch from spatial inhomogeneities in the plasma that change the dispersion relationship of the excited waves as the instability travels through the plasma. If the low-frequency wave is an ion acoustic wave, as is suspected (evidence to be presented later), a temperature gradient along the axis[25] could alter the wave number of the low-frequency wave as it propagates from the excitation region to the probe. Therefore, if the parametric decay occurs near the antenna, wave coherence could be lost by the time the waves propagate 35 cm downstream to the probe location. Note that below rf of 8 MHz, the wave lengths (perpendicular and parallel) of the low-frequency wave decrease sharply (Fig. 6). The lack of wave number conservation in the perpendicular direction at 10 and 11 MHz corresponds to the rapid decrease in the parallel wave number seen at the lower hybrid resonance in Fig. 5. However, we do not have an explanation as to why momentum conservation is broken in the perpendicular direction and not the parallel direction at these rf. Similar results were obtained for other background magnetic-field strengths, i.e., the wave number matching

Downloaded 19 Dec 2002 to 157.182.108.189. Redistribution subject to AIP license or copyright, see http://ojps.aip.org/pop/popcr.jsp

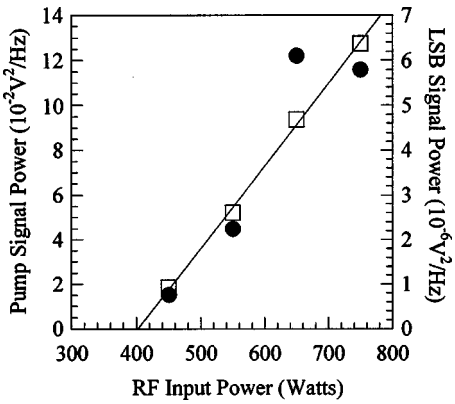

FIG. 8. Peak spectral power of the (●) pump and the (□) lower side band waves versus rf power for an rf of 11 MHz, a magnetic-field strength of 737 Gauss, and a neutral pressure of 6.7 mTorr.

condition is generally satisfied and when the pump frequency drops below the local lower hybrid frequency, the electrostatic side band and low frequency wave lengths decrease.

B. Parametric decay versus rf power

Another key signature of parametric decay is the power coupling between the pump wave and the parametrically driven waves. For fixed coupling strengths between a set of waves and fixed damping rates of the parametrically driven waves, the pump wave amplitude must exceed a threshold before parametric excitation occurs.[24] Figure 8 shows the power in the lower side band and pump wave at four different rf input powers, an rf of 11 MHz, and a magnetic-field strength of 737 G. The peak power in the parametrically excited waves increases linearly with pump power. For typical three-wave parametric decay, the power in the parametrically excited waves should increase exponentially with increasing power in the pump wave.[4,26] However, in this experiment, the same antenna that excites the helicon pump wave is also responsible for generating the plasma. As the input power increases (increasing the amplitude of the pump wave), the plasma parameters change, i.e., density, electron temperature and ion temperature. Therefore, the varying plasma parameters should also change the growth rates of the parametrically excited waves and a detailed theoretical analysis including the interdependencies of the plasma parameters and wave growth rates is required to accurately calculate the expected scaling of power in the parametrically driven waves as a function of pump power. Such a calculation is outside the scope of the present work. However, Fig. 8 does show that a threshold for the parametric decay exists. Parametrically driven, electrostatic waves were not observed for input powers less than 450 Watts, i.e., there is a clear power threshold that is consistent with a classic parametric decay process. For input powers less than 450 Watts, HELIX also drops out of the helicon mode into the inductive mode.[27] Thus, the pump power required to operate the helicon source in the helicon mode exceeds the threshold for parametrically driving the electrostatic waves. If other helicon sources have similar thresholds for helicon mode operation and parametric decay, these measurements suggest that parametric decay should be observable in all helicon sources operating in the helicon mode. There may even be a causal link between parametric decay and the helicon mode transition. In other words, large enough rf powers to drive parametric decay may be required for helicon mode operation.

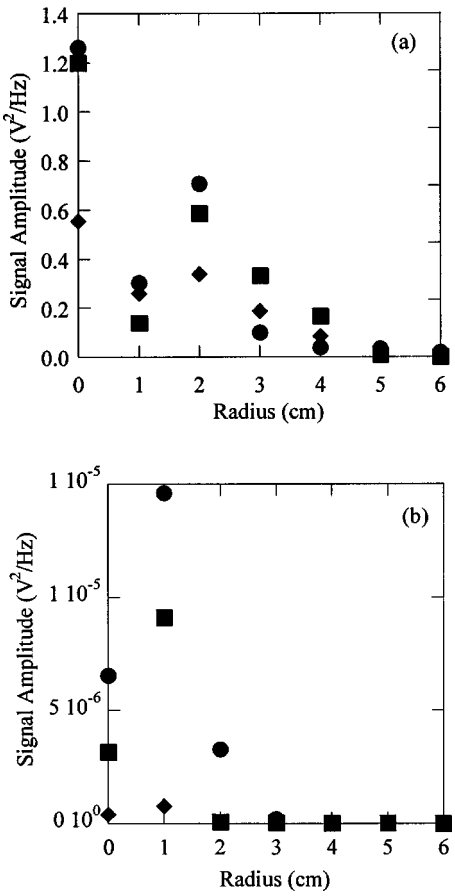

FIG. 9. Peak spectral power of the (a) pump and (b) upper side band waves versus radius at a magnetic-field strength of 910 G and rf of (●) 9 MHz, (■) 11 MHz, and (♦) 13 MHz.

C. Parametric decay versus radial location

The electrostatic fluctuation power spectra were also measured at different radial locations for different rf pump frequencies in HELIX. The peak spectral power in the pump and upper side band waves for three different rf (9, 11, and 13 MHz) and a magnetic field strength of 910 Gauss are shown in Fig. 9 as a function of radial location. For all three rf, the parametrically coupled waves are localized to the center of the helicon source, $r<3$ cm. The rf is slightly below the on-axis lower hybrid frequency for the 9 MHz case, slightly above for the 11 MHz case, and well above for the 13 MHz case. In all three cases, the electrostatic signature of the pump wave is largest on axis [Fig. 9(a)]. However, the on axis power for the 13 MHz case is less than half the power observed for the two lower frequencies even though the input rf power is the same in all three cases. At this magnetic-field strength, higher plasma densities were obtained at 9 and 11 MHz than at 13 MHz.[20] These measurements provide experimental evidence of better power coupling into the plasma waves at lower rf for identical input powers.

Downloaded 19 Dec 2002 to 157.182.108.189. Redistribution subject to AIP license or copyright, see http://ojps.aip.org/pop/popcr.jsp

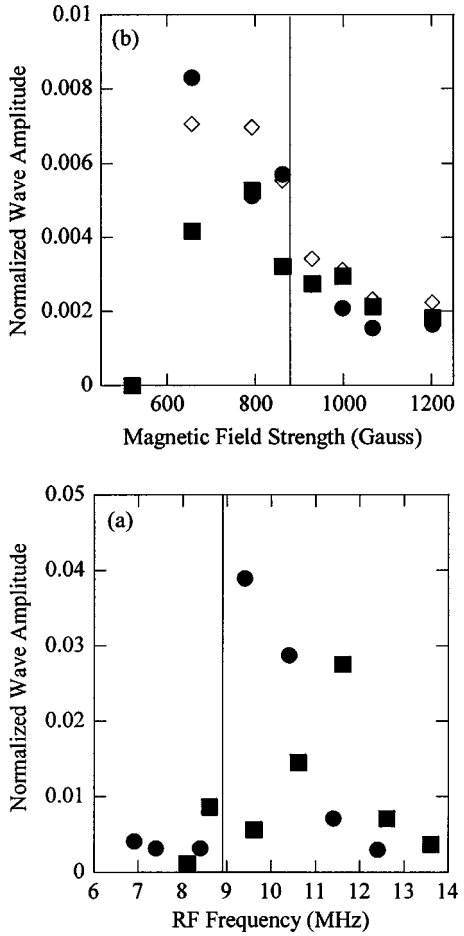

FIG. 10. (a) Normalized amplitudes of (●) the lower side band and (■) the upper side band as a function of rf for a magnetic field of 845 Gauss. (b) Normalized amplitudes of (●) the lower side band, (■) the upper side band, and (◇) low-frequency wave as a function of magnetic-field strength for a rf driving frequency of 9 MHz. The vertical lines indicate where the upper side band frequency matches the lower hybrid frequency.

At $r=1$ cm, the power in at the pump frequency drops sharply for all three frequencies examined. At the same $r=1$ cm radial location, the spectral power in the upper side band wave increases sharply for both the 9 and 11 MHz cases [Fig. 9(b)]. Note that for the 13 MHz case, very little lower side band power is measured at all radii. Across the entire inner region of the plasma, the 9 MHz case exhibits the largest levels of upper side band power [Fig. 9(b)].

D. Parametric coupling versus magnetic field strength and rf

To investigate the parametric coupling strength of the driving wave to the lower hybrid waves verses rf and magnetic field strength, the side band and low frequency wave amplitudes were normalized to the pump wave amplitude to account for amplitude changes in the pump wave. Figure 10(a) shows the power in the side bands as a function of rf for a fixed magnetic-field strength of 845 Gauss. The amplitudes of the side bands are largest when the rf driving frequency is larger than the lower hybrid frequency by a large enough margin such that all three wave (the pump, the lower side band, and the upper side band) frequencies are larger than the lower hybrid frequency. Figure 10(b) shows the normalized wave amplitudes for the lower side band, upper side band, and low-frequency component plotted as a function of magnetic-field strength for a 9 MHz rf driving frequency. Again, the largest coupling occurs when the frequencies of both side bands are above the lower hybrid frequency. The vertical lines in Fig. 10 indicate where the lower side band frequency is equal to the lower hybrid frequency. Similar trends are seen in magnetic field and rf scans at other rf and magnetic-field strengths. In the cold plasma approximation, wave frequencies above the lower hybrid frequency have real perpendicular wave numbers. However, for wave frequencies below the lower hybrid frequency the perpendicular wave numbers are purely imaginary and the waves are strongly damped.[28] Thus, strong coupling to the lower hybrid waves, as seen in Fig. 10, is expected for rf above the lower hybrid frequency.

The power in the sidebands can become large for side band frequencies below the lower hybrid frequency [Fig. 11(a)], but the pump wave amplitude also increases dramatically. Thus, the coupling is weaker for rf below the lower hybrid frequency and it is unclear if the sidebands are lower hybrid quasi modes (strongly damped waves) or another plasma wave. For plasmas with finite electron and ion temperatures, there are a plethora of waves that can propagate near the lower hybrid resonance.[22]

IV. DISCUSSION

That parametrically driven waves appear in helicon sources should not be surprising given the number of previous experiments that have observed parametrically driven waves when similar plasmas are driven with comparable strength rf waves.[7] The electrostatic probe measurements indicate that the power in the parametrically driven waves is largest near the axis of the helicon source. The only electromagnetic wave that can propagate in this region of the helicon source is the helicon wave since the slow or ''Trivelpiece–Gould'' wave is strongly damped at the plasma edge.[29] Akhiezer *et al.*[3] have suggested that damping of the helicon wave by the excitation of parametrically driven ion sound turbulence could explain the helicon wave damping rate and the peak in the plasma density downstream of the rf antenna observed in helicon sources.[30,31] In their model, the short wavelength ion sound turbulence is most efficiently driven for rf near the lower hybrid frequency. The ion sound turbulence scatters electrons, leading to electron heating and increased density production. Such a mechanism would explain the correlation between the lower hybrid frequency and plasma density production in HELIX and would be consistent with a peaked density profile (simple magnetically limited diffusion also yields a centrally peaked density profile). Although the predicted perpendicular wavelengths for the ion sound turbulence are too small to be measured with probes, recent microwave scattering experiments suggest that short wavelength; ion acoustic-like turbulence is generated in helicon sources.[32]

Electron scattering by ion sound turbulence is not the only mechanism whereby parametrically driven waves can

Downloaded 19 Dec 2002 to 157.182.108.189. Redistribution subject to AIP license or copyright, see http://ojps.aip.org/pop/popcr.jsp

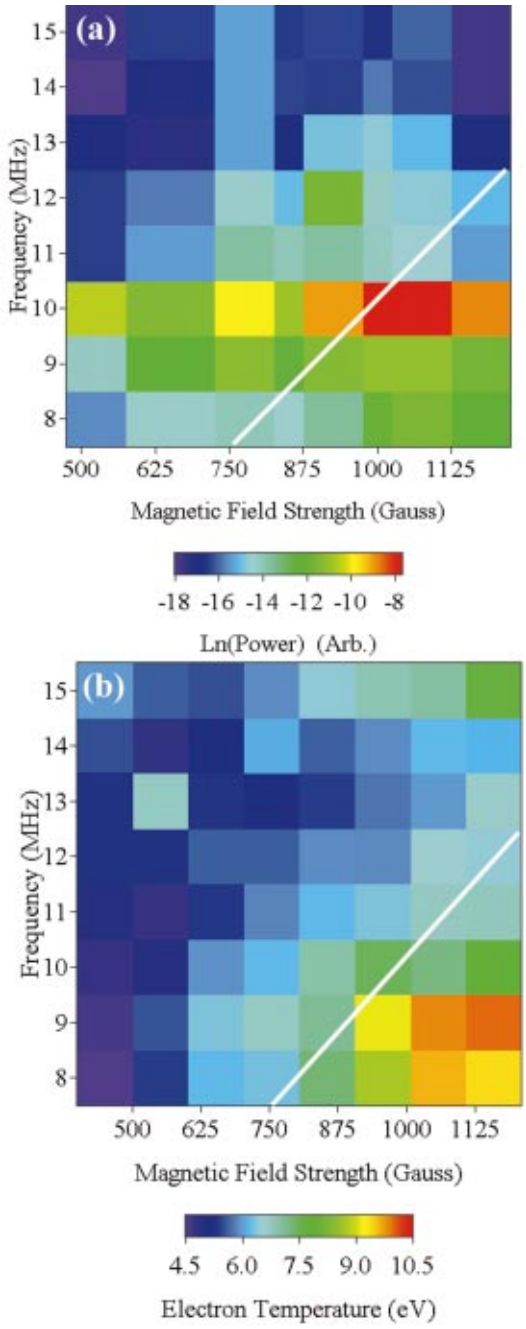

FIG. 11. (Color) (a) Peak spectral power in the electrostatic lower side band wave as a function of magnetic-field strength and rf pump frequency. (b) Electron temperature as a function of magnetic-field strength and rf pump frequency. The white line indicates the parameters at which the rf pump frequency equals the on-axis lower hybrid frequency.

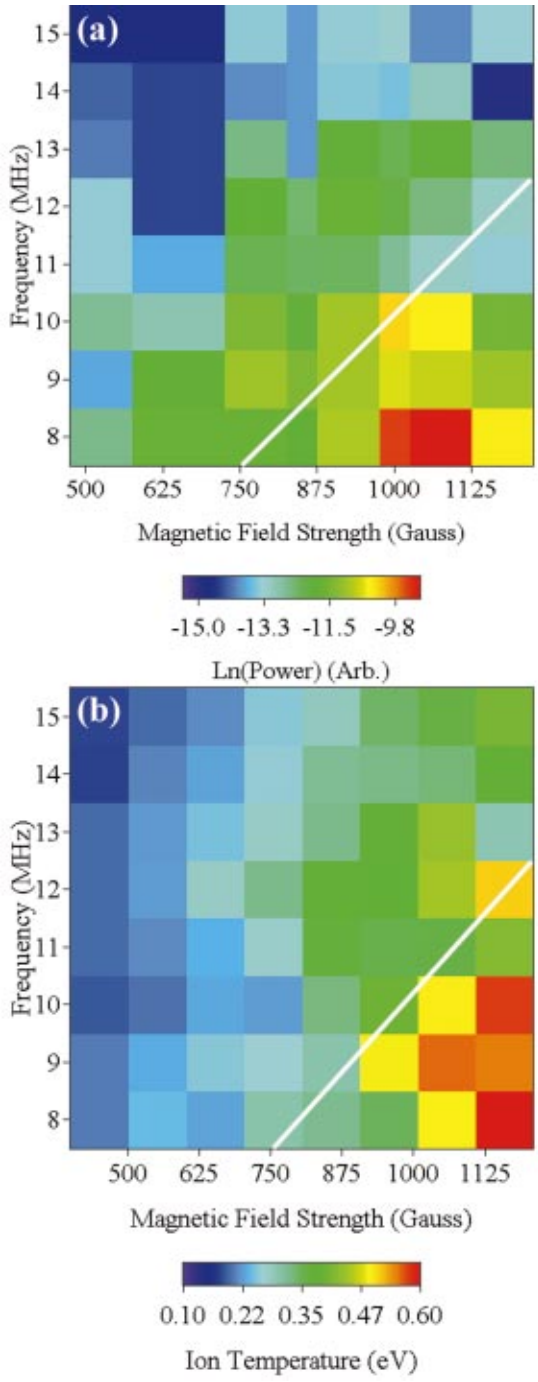

FIG. 12. (Color) (a) Peak spectral power in the low-frequency electrostatic wave as a function of magnetic-field strength and rf pump frequency. (b) Perpendicular ion temperature measured 5 cm in front of the antenna as a function of magnetic-field strength and rf pump frequency. The white line indicates the parameters at which the rf pump frequency equals the on-axis lower hybrid frequency.

couple energy into the plasma particles. To couple wave energy directly into the electrons through Landau damping, the phase velocity of the wave must be near the electron thermal velocity, v_{the}. For the frequency range of 8–11 MHz, the parallel phase speeds, $\omega/k_{\|}$, of the electrostatic lower side band waves are on the order of $2.7\times10^{7}-3.8\times10^{7}$ cm/s, or $0.4-0.8\,v_{\mathrm{the}}$. If the lower side band waves do couple energy directly into the electrons, there should be a correlation between power in the lower side band waves and the measured electron temperature. The power in the lower side band wave and the measured electron temperature are shown in Fig. 11 as a function of magnetic-field strength and rf. Except at the highest rf pump frequencies, the variations in lower side band power and electron temperature as a function of magnetic field strength and rf are qualitatively similar. Both show a strong correlation with the lower hybrid frequency curve and both peak for rf below the lower hybrid frequency. Note that these data are consistent with the previous discussion of the strength of the parametric coupling being largest for rf

Downloaded 19 Dec 2002 to 157.182.108.189. Redistribution subject to AIP license or copyright, see http://ojps.aip.org/pop/popcr.jsp

above the lower hybrid frequency. The parameter of interest in this discussion is the total power in the lower side band waves, not the normalized power shown in Fig. 10. The increase in absolute power in the lower side band wave may simply result from more efficient coupling of rf power into the helicon source via an eigenmode of the system.[17,33] Thus, the increase in helicon wave amplitude increases the absolute energy deposition into the parametrically excited waves and electron heating and density production are correlated with the amplitude of the lower side band wave.

To couple wave energy into the ions, the phase speed of a wave must be close to the ion thermal speed. For wave numbers less than 10 rad/cm (the maximum wave number resolvable with the electrostatic probe), the wave frequency must be below 900 kHz to be less than five times the thermal speed of 0.5 eV ions. Thus, only the low-frequency electrostatic wave could directly couple energy into the ions. Figure 12 shows the power in the low frequency electrostatic wave and the perpendicular ion temperature 5 cm from the front of the rf antenna as a function of magnetic-field strength and rf driving frequency. At high magnetic field strengths, above 900 Gauss, the peak in the amplitude of the low frequency electrostatic wave is well correlated with the peak in the perpendicular ion temperature. Both the perpendicular ion temperature and low-frequency wave power plots have a region of reduced intensity around an rf of 11 MHz and a magnetic-field strength of 1100 Gauss. These observations suggest that near the rf antenna, the parametrically driven low-frequency electrostatic wave either directly heats the ions or is driven by the same mechanism responsible for the ion heating.

As noted previously, the characteristics of the lower and upper side band waves are consistent with expectations for electrostatic lower hybrid waves. If the low frequency, electrostatic wave observed in these experiments is an azimuthally propagating ion acoustic wave, the measured wave phase speed (ω/k) should equal the ion sound speed, $c_s \sim(\gamma k_b T_e/m_i)^{1/2}$ for $T_e > T_i$ where k_b is Boltzmann's constant, m_i is the ion mass, and γ is the ratio of specific heats. The electron temperatures calculated from the measured wave phase speeds, $T_e = m_i\omega^2/\gamma k_b k^2$ with $\gamma=5/3$, are shown in Fig. 13 along with the electron temperatures measured on axis with the Langmuir probe as a function of rf. Except at 13 MHz, the measured electron temperatures are consistent with the calculated electron temperatures assuming the wave is an ion acoustic wave. The dotted lines in Fig. 13 also show the electron temperatures calculated from the sound speed for $\gamma=1$ and $\gamma=2$. The $\gamma=2$ calculated temperatures are in better agreement with the Lagnmuir probe measured electron temperatures while the calculations for $\gamma=1$ (an isothermal plasma) are not. For a plasma to be isothermal, the electrons must be free to move multiple wave lengths in one wave period. It is true that the phase speed of the parametrically excited waves is less than the electron thermal speed. However, for an argon neutral pressure of 6.8 mTorr and electron temperature of 6 eV the electron-neutral mean free is 2.5 cm—on the order of the wavelength for the parametrically excited waves. Therefore, the electrons should not be expected to act isothermally.[34] γ greater than one is consistent

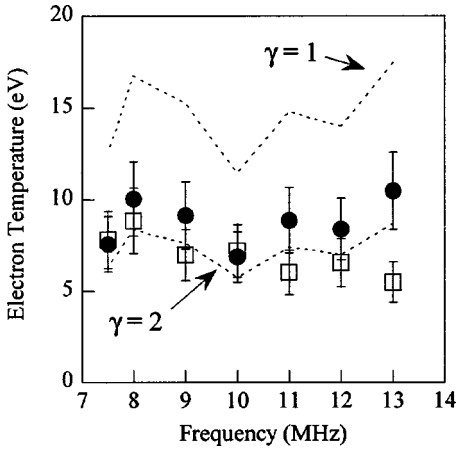

FIG. 13. Electron temperatures measured with the rf compensated Langmuir probe (□) and calculated for an ion acoustic wave propagating at the measured wave phase speeds (●).

with other experimental results that show the existence of electron and ion temperature gradients in helicon plasmas with similar parameters.[15,20,25] So although the plasma is also not adiabatic, a choice for the ratio of specific heats between $\gamma=5/3$ and $\gamma=2$ (independent perpendicular and parallel degrees of freedom) is reasonable given the experimental data, and the low-frequency wave is very likely an ion acoustic wave.

Since the low frequency wave is polarized perpendicular to the magnetic field, it is possible that the low-frequency wave could be a backwards propagating cyclotron wave (with phase and group velocities in opposite direction), but in the fluid limit ($k\lambda_D \ll 1$ where λ_D is the Debye length) the only difference in the dispersion relationship between a cyclotron wave and an ion acoustic wave is the addition of the cyclotron frequency as a constant. The additional ion cyclotron frequency term slightly reduces the calculated electron temperatures in Fig. 13, yielding even better agreement with the Langmuir probe measurements.

V. CONCLUSIONS

Parametric decay of the helicon wave into two electrostatic waves has been observed in a helicon source. The measurements are consistent with the parametric excitation of a lower hybrid wave and an ion acoustic wave. The parametric coupling is strongest for rf above the lower hybrid frequency. Since intense downstream ion heating occurs for rf below the lower hybrid frequency,[20] these parametrically excited waves are not likely to be responsible for downstream ion heating in helicon sources. However, a correlation between the amplitude of the lower hybrid wave and electron temperatures and a correlation between the amplitude of the ion acoustic wave and ion temperatures near the antenna are also observed. Since the parametrically excited waves can interact with the electrons (and ions), providing an alternative means for the helicon wave to deposit energy in the plasma, parametric processes could play an important role in the energy balance of and rf absorption in helicon sources. These measurements demonstrate that nonlinear processes such as para-

Downloaded 19 Dec 2002 to 157.182.108.189. Redistribution subject to AIP license or copyright, see http://ojps.aip.org/pop/popcr.jsp

metric decay must be included in models of helicon source physics if rf absorption in helicon sources is to be completely understood.

ACKNOWLEDGMENTS

We would like to thank the members of the WVU machine shop, Doug Mathess, Tom Milan, and Carl Weber, for all of their efforts contributing to the work done by the WVU Helicon group. We also acknowledge David Montgomery of Los Alamos National Laboratory and Vladimir Mikhailenko of Kharkov National University for useful discussions during the preparation of this manuscript, and Paul Keiter for writing the first version of the fluctuation analysis software.

Work at WVU was performed with support from National Science Foundation Grant No. ATM-99988450 and the U.S. Department of Energy under Grant No. DE-FG02-97ER54420.

[1]V. F. Virko, G. S. Kirichenko, and K. P. Shamrai, Plasma Sources Sci. Technol. **11**, 10 (2002).
[2]M. Light, F. F. Chen, and P. L. Colestock, Phys. Plasmas **8**, 4675 (2001).
[3]A. I. Akhiezer, V. S. Mikhailenko, and K. N. Stepanov, Phys. Lett. A **245**, 117 (1998).
[4]M. Porkolab, V. Arunasalam, and R. A. Ellis, Jr., Phys. Rev. Lett. **29**, 1438 (1972).
[5]M. Porkolab, V. Arunasalam, and B. Grek, *International Congress on Waves and Instabilities in Plasmas* (Innsbruck, Austria, 1973).
[6]M. Porkolab, Phys. Fluids **20**, 2058 (1977).
[7]K. L. Wong and M. Ono, Phys. Rev. Lett. **47**, 842 (1981).
[8]R. W. Boswell, Phys. Lett. **55A**, 93 (1975).
[9]E. E. Scime, P. A. Keiter, M. M. Balkey *et al.*, Phys. Plasmas **7**, 2157 (2000).
[10]J. L. Kline, Ph.D. dissertation West Virginia University (2002).
[11]I. D. Sudit and F. F. Chen, Plasma Sources Sci. Technol. **3**, 162 (1994).
[12]R. A. Stern and J. A. Johnson, III, Phys. Rev. Lett. **34**, 1548 (1975).
[13]D. H. Hill, S. Fornaca, and M. G. Wickham, Rev. Sci. Instrum. **54**, 309 (1983).
[14]E. E. Scime, P. A. Keiter, M. W. Zintl *et al.*, Plasma Sources Sci. Technol. **7**, 186 (1998).
[15]J. L. Kline, E. Scime, R. Boivin, A. M. Keesee, and X. Sun, Plasma Sources Sci. Technol. **11**, 413 (2002).
[16]P. K. Loewenhardt, B. D. Blackwell, and Zhang Beichao, Rev. Sci. Instrum. **64**, 3334 (1993).
[17]M. Light, I. D. Sudit, F. F. Chen *et al.*, Phys. Plasmas **2**, 4094 (1995).
[18]J. M. Beall, Y. C. Kim, and E. J. Powers, J. Appl. Phys. **53**, 3933 (1982).
[19]R. W. Boswell, Plasma Phys. Controlled Fusion **26**, 1147 (1984).
[20]J. L. Kline, E. E. Scime, R. F. Boivin *et al.*, Phys. Rev. Lett. **88**, 105002 (2002).
[21]D. G. Swanson, *Plasma Waves*, 1st ed. (Academic, Boston, 1989).
[22]T. H. Stix, Phys. Rev. Lett. **15**, 878 (1965).
[23]M. N. Rosenbluth, Phys. Rev. Lett. **29**, 565 (1972).
[24]K. Mima and K. Nishikawa, in *Handbook of Plasma Physics*, edited by M. N. Rosenbluth and R. Z. Sagdeev (North-Holland, Amsterdam, 1984).
[25]I. D. Sudit and F. F. Chen, Plasma Sources Sci. Technol. **5**, 43 (1996).
[26]E. Albers, K. Krause, and H. Schluter, Plasma Phys. **21**, 193 (1979).
[27]A. R. Ellingboe and R. W. Boswell, Phys. Plasmas **3**, 2797 (1996).
[28]T. H. Stix, *Waves in Plasmas* (AIP, New York, 1992).
[29]F. F. Chen and D. Arnush, Phys. Plasmas **4**, 3411 (1997).
[30]F. F. Chen, Phys. Plasmas **3**, 1783 (1996).
[31]F. F. Chen, I. D. Sudit, and M. Light, Plasma Sources Sci. Technol. **5**, 173 (1996).
[32]N. M. Kaganskaya, M. Krämer, and V. L. Selenin, Phys. Plasmas **8**, 4694 (2001).
[33]G. G. Borg and R. W. Boswell, Phys. Plasmas **5**, 564 (1998).
[34]N. A. Krall and A. W. Trivelpiece, *Principles of Plasma Physics* (San Francisco Press, San Francisco, 1986).

Downloaded 19 Dec 2002 to 157.182.108.189. Redistribution subject to AIP license or copyright, see http://ojps.aip.org/pop/popcr.jsp